High-Fidelity Analysis of Propeller-Rudder System Acoustic Signatures in a Full-Scale Marine Vessel: Underwater Radiated Noise Spectra from Wake Structures and Cavitation

M.R. Pendar *, D. McIntyre and P. Oshkai

Dept. of Mechanical Engineering, the University of Victoria, Canada

* Correspondent author: pendar@uvic.ca

Abstract

The use of computational fluid dynamics (CFD) to predict the acoustic signature of marine propellers operating in highly turbulent and non-uniform flow conditions has attracted considerable academic and industrial interest over the past decade. The negative effects of radiated noise from underwater maritime and shipping activities on marine ecosystems and aquatic life are well recognized. This noise originates from various sources, mainly vessel propellers operating. This study aims to characterize the noise levels generated by marine vessels through high-fidelity numerical modeling of hydroacoustic phenomena. We employed Large Eddy Simulations (LES), the Kunz cavitation modeling approach, and the compressive Volume of Fluid (VOF) method to simulate cavitating flow over the propeller and predict the far-field radiated noise using the Ffowcs Williams-Hawkings (FW-H) hydroacoustic analogy. This study provides insights into the flow physics of noise generation due to wake structures—such as tip, root, trailing edge, and hub—and cavitation patterns, including sheet, tip, and hub cavitation, over marine propellers operating upstream of a rudder. We characterized the instability of vortical structures in the wake of the marine propeller, including tip/hub vortex oscillation and instability, mutual-inductance instability (leapfrogging effect), elliptic instability, and first and second wake grouping. Additionally, we examined sound levels related to propeller loading, cavitation development, periodic pulsating cavitation, and pressure fluctuations in both the near-field and far-field. Finally, the comparison between modeled and measured noise provided insights into the spectral contributions of propeller- and non-propeller-generated noise, helping to define the range of applicability for the assumption that propeller sources dominate overall noise emissions from the vessel.

Keyword: *Hydroacoustic Analysis, Wake Structure, Cavitation-Induced Noise, Large-eddy simulation (LES), Ffowcs Williams-Hawkings (FW-H)*

1. Introduction

The overall level of noise produced by marine vessels has been increasing, adversely affecting the soundscape of aquatic environments [1, 2]. There is a noticeable trend toward using more standardized vessels to enhance ecological protection, as well as an assessment of the impacts of shipping noise on marine ecology [3, 4]. To foster a synergistic relationship between vessel-generated noise and marine aquatic ecology, it is essential to conduct a thorough investigation of the underwater radiated noise (URN) characteristics of ships and develop models for the source spectrum.

Gassmann et al. [5] and McKenna et al. [6] monitored URN from various types of commercial vessels, including container ships, bulk carriers, tankers, and vehicle carriers, under standard operating conditions. They also measured deep-water noise generated by container ships. Analysis of the monitoring data showed that the broadband source levels (SL) of URN from vessels primarily ranged from 150 to 180 dB, with most source frequencies concentrated below 1 kHz.

Significant changes in propeller design, particularly for modern ships, have resulted in variations in the types of underwater sound sources, with propellers being a major contributor to underwater radiated noise (URN) [7]. The average SL of a specific vessel is modeled as a function of speed (V), ship length (L), and frequency (f) [8]. ROSS [9], W&H [10], and RANDI [11] are classical models for estimating URN from ships based on the measured data in various periods. The ROSS model measures the URN from cargo ships and accurately quantifies the noise source spectrum levels produced by seagoing vessels. The proposed W&H model addresses and corrects the overestimation of source spectra found in the ROSS model. The RANDI-2 model improves the understanding of variations in URN from ships within the frequency range of 70 to 700 Hz.

Differences in vessel designs, bathymetry characteristics, and related URN have led to limitations in classical model predictions, increasing the reliance on CFD modeling and dependent acoustic models. Currently, three approaches are used for noise prediction in numerical modeling: Lighthill’s acoustic analogy, computational aeroacoustics (CAA), and semi-empirical models. In this study, the Ffowcs Williams-Hawkings (FW-H) equation, which is known for its efficiency and is based on Lighthill’s acoustic theory, is utilized [3].

The noise generated by ship propellers, especially in the cavitation regime within highly turbulent wakes [12], leads to pressure fluctuations and prominent acoustic characteristics. Here, we aim to characterize noise levels by analyzing the acoustic signatures produced by marine vessels through high-fidelity numerical hydro-acoustic modeling.

2. Simulation Methodology

2.1 Governing equations

In this study, the high-fidelity Large Eddy Simulation (LES) turbulence model is used, which involves computing large, energy-containing eddies that are resolved on the computational grid, while the smaller, more isotropic sub-grid structures are modelled [13]. The homogeneous multiphase incompressible Navier-Stokes (NS) equations are employed using Favre-filtering. Here, subgrid-scale terms are modeled using the "one equation eddy viscosity" model [14].

A conservative transport equation based on the Volume of Fluid (VOF) method, implemented within the OpenFOAM framework, is used to track the interface of vapor cavities [15], while the Schnerr and Sauer models utilize a mass transfer approach [16]. Finally, the Ffowcs Williams-Hawkings (FW-H) acoustic analogy is used to compute the far-field radiated noise [3].

2.2 Problem Description

Fig. 1 schematically illustrates the geometry of the considered problem (propeller/rudder system), the boundary conditions, constructed grids over the computational domain, microphone Positions, the solution method, and the sequential stages of the optimization-driven framework employed in the present study. The computational domain was defined by employing suitable boundary conditions, dimensions, and a fully refined, high-quality mesh encompassing the rotor and the stator subdomains. The propeller used in this study is the INSEAN E779A with $D_{\text{Propeller}}$= 0.227m, which is characterized by its four blades. The rudder, a hydrofoil with a NACA0015 profile, is located downstream of the propeller. A time step size 4.5×10^{-5}, resulting in a Courant–Friedrichs–Lewy number of 0.2. The accuracy of the employed code and of the overall numerical strategy was assessed during the validation phase. Key variations in constructing the desired realistic operational conditions included adjustments to the free-stream velocity, the rotational speed of the propeller, the Reynolds number, the advance coefficient, and the cavitation number. To quantify the flow characteristics, microphones are arranged around the computational domain, over the propeller blade, and along the rudder surface. The total number of mesh elements, 14.1 million, was generated using the SnappyHexMesh tool with the Cyclic-Arbitrary Mesh Interface (Cyclic-AMI) technique and meets the LES requirements for grid resolution following a grid independence analysis [3]. The simulations were conducted in a high-performance computing environment. For example, the total computational time was approximately 860 hours using 144 parallel processor cores.

The analysis primarily involved monitoring the wake structure characteristics, the performance parameters of the propeller (such as torque and thrust coefficients), and detecting the noise sources. Subsequently, acoustic analysis was conducted in depth utilizing the computed pressure distribution.

2.3 Validation

Here, the precision of the code is evaluated for validation purposes. Fig. 2 (a, b) compares the vortical structures obtained in this work, using the Q-criterion, with the experimental snapshots reported by Felli et al. [17]. There is a strong qualitative resemblance to the experimental results, accurately capturing features such as tip/hub vortex instability, mutual inductance, elliptic instabilities, and the first and second wake groupings. In Fig. 2(c), the thrust and torque coefficients for a specific advance coefficient (J = 0.75), obtained through our numerical modeling for the E779A propeller, are compared with the experimental data reported by Felli et al. [17]. A good agreement is observed, with the predicted coefficients having an error of less than 2%.

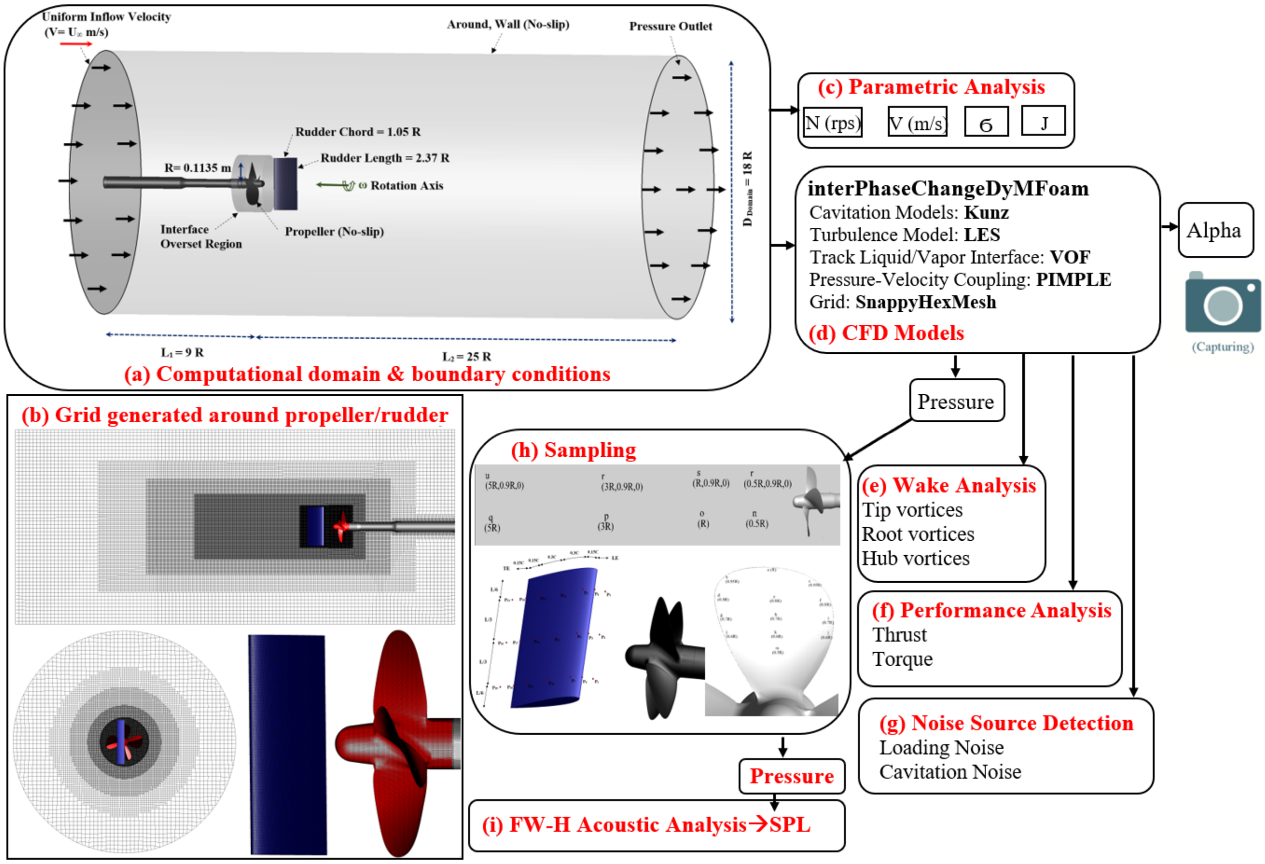

Fig. 1 Schematic diagram of the solution procedure.

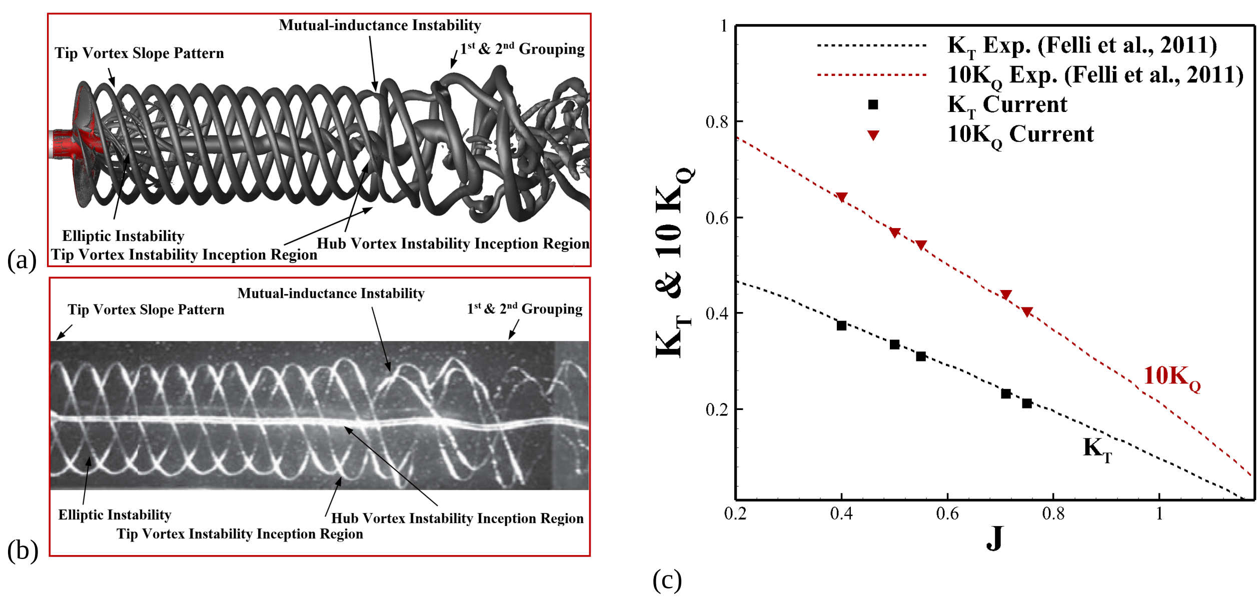

Fig. 2 (a, b) Comparison of the propeller wake between our numerical results and the experimental snapshots from Felli et al. [17] (advance ratio = 0.75). (c) Comparison of thrust and torque coefficients for the E779A propeller with the experimental data from Felli et al. [17].

3. Results and Discussions

Fig. 3(a) illustrates the non-machinery radiated noise sources generated by marine vessels. At full ship speed, At the ship's maximum speed, propeller noise is the dominant source across most of the frequency spectrum. At lower speeds, the noise signature is characterized by machinery-induced noise in the low to mid-frequency range and propeller vortex shedding and turbulence ingestion in the mid to high-frequency range. In contrast, fluid-solid interactions caused by flow over the ship's hull or wave motion generate relatively low noise levels compared to other typical noise sources on vessels, as further explained in Fig. 4. Fig. 3(b) depicts the design loop for a ship, where meeting acoustic criteria (noise and vibration levels) is a critical consideration. Acoustic limits significantly depend on the vessel type, function, and operational conditions (e.g., full speed, station keeping). The designer may employ optimization techniques for treatment to reduce noise levels in existing vessels or to improve the design of new vessels.

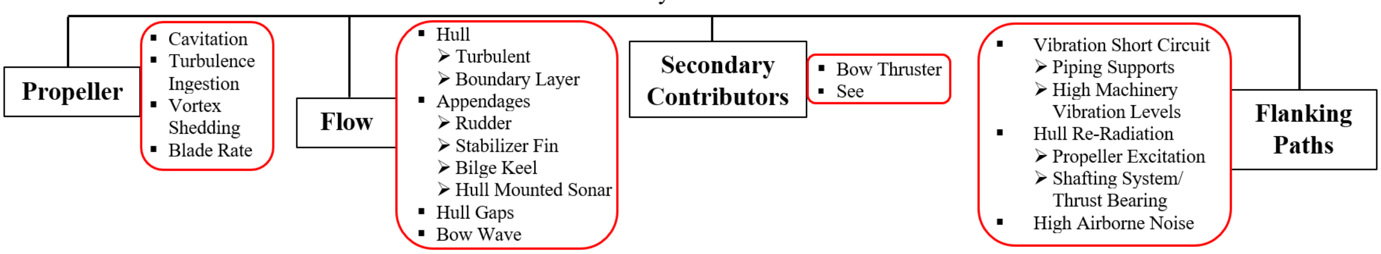

(a)

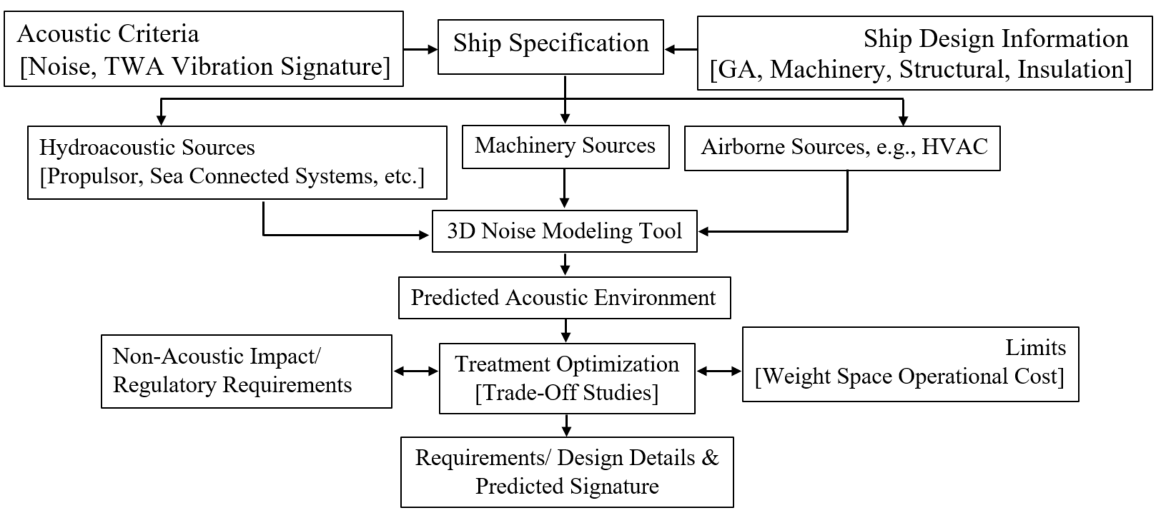

(b)

Fig. 3 (a) Summary of non-machinery radiated noise sources, (b) progressive steps for ship design loop.

Figs. 4 and 5 compares the formation of wake fields using Q-criterion iso-surfaces, colored by vorticity, pressure coefficient, and velocity magnitude, over the propeller at various advance coefficients (J) and different rudder maneuvering angles (α). Wake patterns consisting of root, tip, hub, and trailing edge vortices form differently due to the rotation of the propeller with increments of α or J. The turbulence destabilization, wake instability, fluctuations, vortex break up, and expansion accelerate downstream of the rudder as the α or J increases. The wake flow features are short-lived and exhibit a dense, irregular, and turbulent pattern, with higher pressures and increased rise across the span observed when the rudder angle or advance coefficient is increased. Hub vortices create areas of local pressure minima, making them more prone to cavitation and the generation of associated noise.

Fig. 6 shows the vapor volume fraction iso-surfaces for the cases considered in Fig. 4. Over the forward propeller, from the leading edge to the tip, and on the rudder, sheet cavitation manifests with higher shedding and collapse rates at increased α or J. This results in elevated monopole sound pressure and intense cavity noise. These effects occur because the local cavitation volume undergoes more rapid changes, causing significant vapor volume acceleration and generating strong acoustic monopole sources.

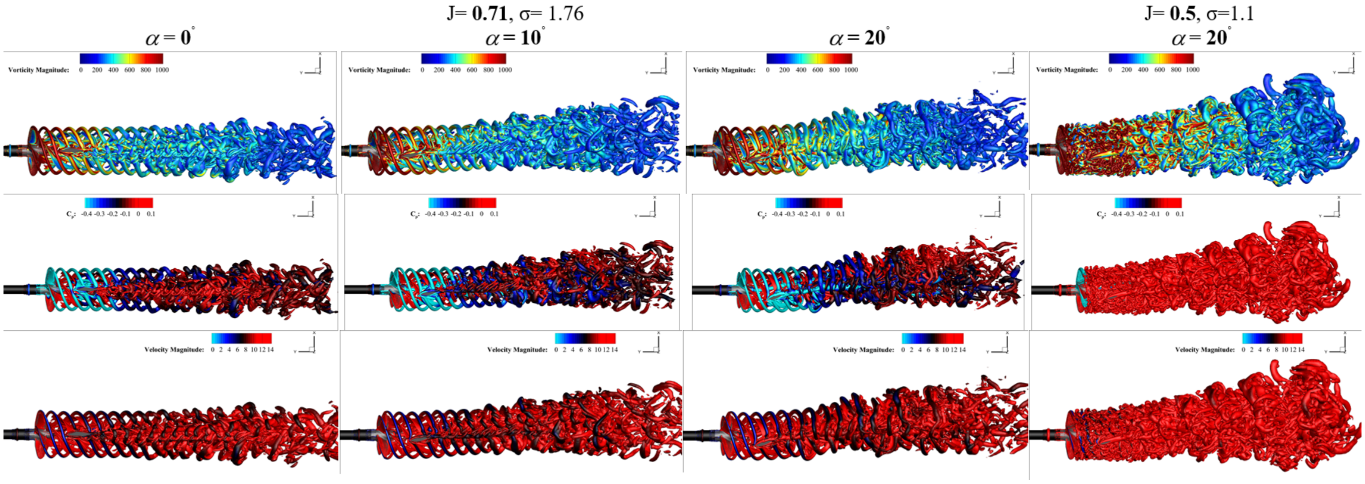

Fig. 4 Comparison of the propeller wake between our numerical results and the experimental snapshots from Felli et al. [17] (advance ratio = 0.75). (c) Comparison of thrust and torque coefficients for the E779A.

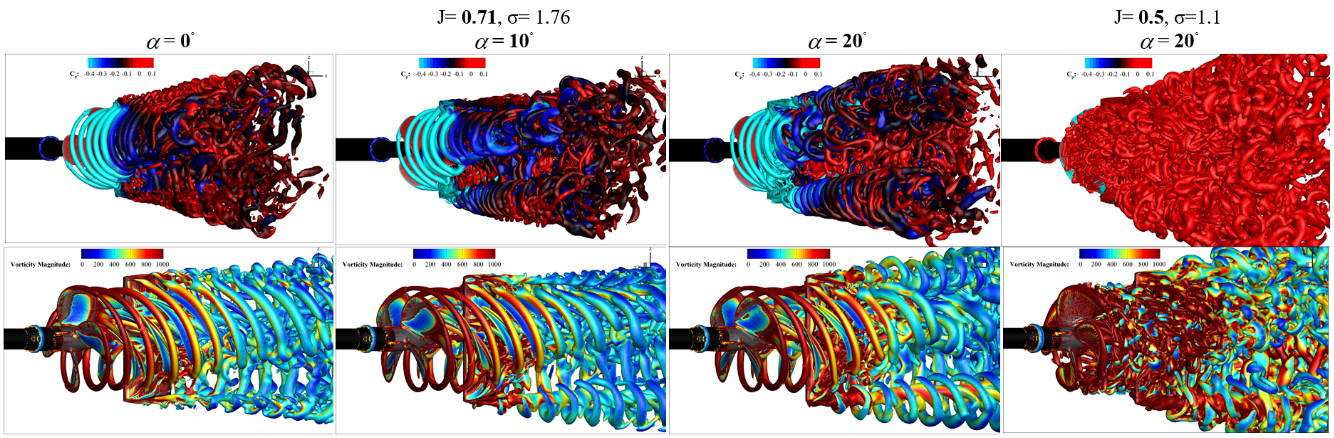

Fig. 5 Back and front views of helical structures using iso-surfaces Q-criterion for introduced cases in Fig. 4.

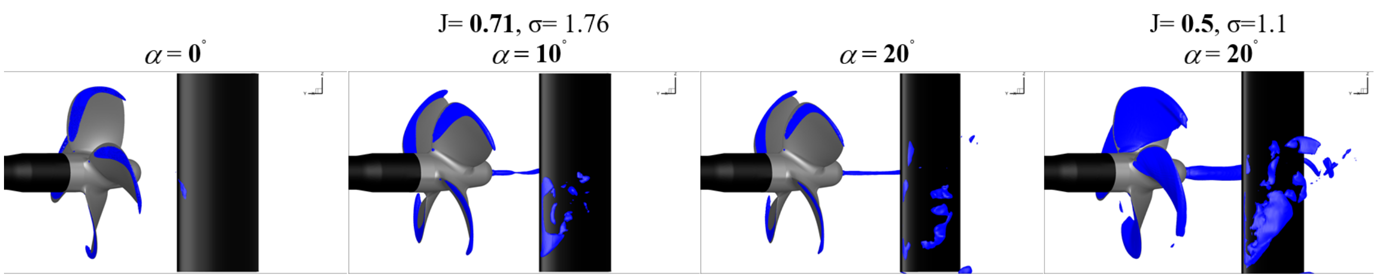

Fig. 6 Evolution of the formed cavitation pattern over the propeller/ rudder surfaces for the cases considered in Fig. 4.

Fig. 7 presents a histogram illustrating the overall sound pressure level (OSPL) at specified microphone positions along the axial distance downstream of the propeller/rudder system and over the rudder's suction side surface. The OSPL shows a nonlinear decrease with increasing distance, attributed to the diminishing flow gradient. As the deflection angle increases, the OSPL becomes higher due to more complex small-scale and multi-rotating vortex structures, leading to the development of vortices across the span with significant dynamic behaviors. For various listeners, the sound levels over the rudder follow similar trends, becoming notably louder with an increased α. A comparison between the OSPL obtained from high-fidelity LES modeling and the FW-H method indicates slightly higher values for LES across almost all microphones.

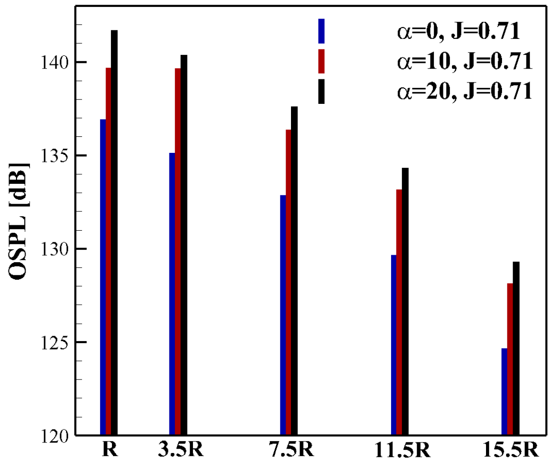

(a)

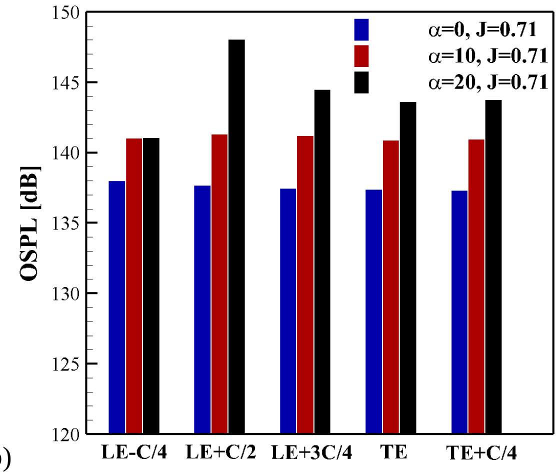

(b)

Fig. 7 Comparison of the overall sound pressure levels (OSPL) for the cases introduced in Fig. 4: (a) at different microphone positions along axial direction and (b) over the suction side surface of the rudder.

4. Conclusion

A high-fidelity numerical analysis of a marine propeller in combination with rudder was conducted to characterize turbulent wake structures under cavitating flow conditions, with the objective of identifying hydro-acoustic noise sources. The primary wake structures—hub, tip, root, and trailing edge—were analyzed across stable, transient, and unstable flow regimes past the propeller, exhibiting behaviors such as smaller scale and short-lived vortices, oscillation, breakup, swirling flow, and helical expansion. Cavitation structures—sheet, tip, and hub—were accurately captured using Large Eddy Simulation (LES) and Sauer cavitation models, revealing their contribution to noise generation. An analysis of pressure fluctuations downstream of the propeller and over the rudder surface showed a significant increase in overall sound pressure level (OSPL) during conditions of high rudder deflection angle or blade loading. This intensification is attributed to the interaction of vortical structures and the development of cavitation.

References

[1] Jalkanen, J.P., Johansson, L., Liefvendahl, M., Bensow, R., Sigray, P., Östberg, M., Karasalo, I., Andersson, M., Peltonen, H. and Pajala, J., 2018. Modelling of ships as a source of underwater noise. Ocean Science, 14(6), pp.1373-1383.

[2] Sakai, M., Haga, R., Tsuchiya, T., Akamatsu, T. and Umeda, N., 2023. Statistical analysis of measured underwater radiated noise from merchant ships using ship operational and design parameters. The Journal of the Acoustical Society of America, 154(2), pp.1095-1105.

[3] Pendar, M.R., McIntyre, D. and Oshkai, P., 2024. Hydroacoustic analysis of a full-scale marine vessel: Prediction of the cavitation-induced underwater radiated noise using large eddy simulations. Physics of Fluids, 36(7).

[4] van Geel, N.C., Risch, D. and Wittich, A., 2022. A brief overview of current approaches for underwater sound analysis and reporting. Marine Pollution Bulletin, 178, p.113610.

[5] Gassmann, M., Wiggins, S.M. and Hildebrand, J.A., 2017. Deep-water measurements of container ship radiated noise signatures and directionality. The journal of the acoustical society of America, 142(3), pp.1563-1574.

[6] McKenna, M.F., Ross, D., Wiggins, S.M. and Hildebrand, J.A., 2012. Underwater radiated noise from modern commercial ships. The Journal of the Acoustical Society of America, 131(1), pp.92-103.

[7] Smith, T.A. and Rigby, J., 2022. Underwater radiated noise from marine vessels: A review of noise reduction methods and technology. Ocean Engineering, 266, p.112863.

[8] Hamson, R.M., 1997. The modelling of ambient noise due to shipping and wind sources in complex environments. Applied Acoustics, 51(3), pp.251-287.

[9] Ross, D., 2013. Mechanics of underwater noise. Elsevier.

[10] Wales, S.C. and Heitmeyer, R.M., 2002. An ensemble source spectra model for merchant ship-radiated noise. The Journal of the Acoustical Society of America, 111(3), pp.1211-1231.

[11] Scrimger, P. and Heitmeyer, R.M., 1991. Acoustic source-level measurements for a variety of merchant ships. the Journal of the Acoustical Society of America, 89(2), pp.691-699.

[12] Pendar, M.R., Cândido, S. and Páscoa, J.C., 2023. Optimization of painting efficiency applying unique techniques of high-voltage conductors and nitrotherm spray: Developing deep learning models using computational fluid dynamics dataset. Physics of Fluids, 35(7).

[13] Pendar, M.R. and Pascoa, J., 2021. Study of the Plasma Actuator Effect on the Flow Characteristics of an Airfoil:

An LES Investigation. SAE International Journal of Advances and Current Practices in Mobility, (2021-01-0016), pp.1206-1215.

[14] Pendar, M.R., Alavi, A. and Roohi, E., 2023. Identification of frequency modes and spectral content for noise suppression: Cavitation flow over 3-D hydrofoil with sinusoidal leading edge. International Journal of Modern Physics C, 34(06), p.2350074.

[15] Pendar, M.R. and Roohi, E., 2015, May. Investigation of cavitation around disk and conical cavitators using different sets of turbulence and cavitation models. In 4th International Conference on Advances in Mechanical Engineering-ICAME (pp. 13-15).

[16] Pendar, M.R., Páscoa, J. and Roohi, E., 2021, May. Cavitating flow structure and noise suppression analysis of a hydrofoil with wavy leading edges. In 11th International Symposium on Cavitation CAV2021 (pp. 10-13).

[17] Felli, M., Camussi, R. and Di Felice, F., 2011. Mechanisms of evolution of the propeller wake in the transition and far fields. Journal of Fluid Mechanics, 682, pp.5-53.